

Ursolic Acid Inhibits Breast Tumor Growth and Angiogenesis through Suppression the Expression of Multiple Adhesion Factors

Xing Ji¹, Kai He^{2,*}

¹ Department of Pharmacology, School of Medicine, Hangzhou City University, 310015 Hangzhou, Zhejiang, China

² Chinese Medicine Pharmacy, The First Affiliated Hospital, College of Medicine, Zhejiang University, 310058 Hangzhou, Zhejiang, China

DOI: <https://doi.org/10.62767/jecacm602.2688>

Keywords

Ursolic acid
Breast cancer
Angiogenesis
Metastasis
4T1 cells
Endothelial cells
Tumor perfusion

* Correspondence

Kai He
Chinese Medicine Pharmacy, The First
Affiliated Hospital, College of Medicine,
Zhejiang University, 310058 Hangzhou,
Zhejiang, China
E-mail: 1503033@zju.edu.cn

Received: 10 April 2025

Revised: 24 April 2025

Accepted: 21 June 2025

Published: 30 June 2025

*Journal of Experimental and Clinical
Application of Chinese Medicine* 2025; 6(2):
52-62.

Abstract

Ursolic acid (UA), a natural pentacyclic triterpenoid, has been reported to exert anti-cancer and anti-angiogenic effects. However, its role in suppressing breast cancer metastasis through modulation of endothelial function and tumor microcirculation remains to be fully elucidated. In this study, we investigated the anti-tumor and anti-angiogenic effects of UA using both *in vitro* assays and an orthotopic mouse model of breast cancer. Cell viability, apoptosis, and cell cycle arrest were assessed in 4T1 cells. Tube formation assays were performed using HUVECs. Tumor progression, blood perfusion, and metastasis were evaluated *in vivo* using bioluminescence imaging, laser Doppler perfusion imaging (LDPI), and histological analyses. UA significantly inhibited 4T1 cell proliferation, induced G1-phase cell cycle arrest, and promoted apoptosis in a dose-dependent manner. *In vivo*, UA reduced tumor growth and metastasis, as evidenced by decreased bioluminescence signals and fewer metastatic lung lesions. UA also suppressed angiogenesis by inhibiting HUVEC tube formation and reducing local tumor perfusion in 4T1-bearing mice. Immunohistochemistry revealed that UA downregulated the expression of key adhesion- and angiogenesis-related molecules, including integrin $\beta 5$, ESM-1, and ICAM-1, in both lung and tumor tissues. These findings demonstrate that UA effectively inhibits breast cancer progression and metastasis by targeting both tumor cells and endothelial function. Its ability to suppress angiogenesis and reduce adhesion molecule expression suggests UA is a promising candidate for anti-metastatic therapy in breast cancer.



1 Introduction

Metastatic breast cancer is the second leading cause of cancer-related deaths among women, with an estimated 39,620 fatalities in the United States in 2013. Despite ongoing declines in breast cancer incidence and mortality rates, the survival rate for metastatic cases remains low [1-3]. Conventional treatments, including surgery, radiotherapy, and chemotherapy, have shown limited efficacy in eradicating metastatic breast cancer [4-6]. This underscores the urgent need for novel therapeutic strategies.

Angiogenesis, the process of forming new blood vessels from preexisting ones, is a crucial factor in cancer progression. Growing evidence suggests that angiogenesis is not only significant in hematologic malignancies but also plays a vital role in tumor growth, invasion, and metastasis [7]. Although the precise mechanisms of pathological angiogenesis remain unclear, research suggests that an imbalance between angiogenic stimulators and inhibitors drives this process. When endothelial cells receive pro-angiogenic signals, they activate and release enzymes that degrade the extracellular matrix, facilitating cell migration, proliferation, and eventual differentiation into new capillaries. Targeting any of these steps presents a potential avenue for therapeutic intervention in angiogenesis-dependent diseases [8].

Ursolic acid (UA), a pentacyclic triterpene acid found in numerous Chinese medicinal herbs, exhibits a wide range of pharmacological effects, including anti-inflammatory, hepatoprotective, antiviral, antioxidant, cytotoxic, antitumor, anti-angiogenic, and anti-metastatic properties [9-13]. Some studies have highlighted the inhibitory effects of UA in the chorioallantoic membrane (CAM) assay [14], as well as its differential influence on endothelial cell proliferation and angiogenesis [15].

In our previous research, we employed a stage IV breast cancer mouse model (4T1 tumor-bearing BALB/c mice) to assess the anti-metastatic potential of UA [16]. 4T1 cells, originating from a spontaneous mammary tumor in BALB/c mice, exhibit aggressive growth when implanted into the mammary fat pad of syngeneic mice and readily metastasize to the lungs, liver, bones, and brain [17,18]. In this report, laser Doppler imager (LDI) was used for measuring blood perfusion of the tumor bearing area, which could measure the local blood and vascular network perfusion and reflect the angiogenic activity of the tumor bearing mice indirectly. Our study demonstrated that ursolic acid exerts dual inhibitory effects on both tumor cells and vascular endothelium, significantly suppressing breast cancer growth, metastasis, and angiogenesis, thereby highlighting its potential as a promising anti-metastatic therapeutic agent.

2 Methods

2.1 Cell culture and animals

Human umbilical vein endothelial cells (HUVECs) were cultured in RPMI 1640 medium (Invitrogen, Carlsbad, CA, USA) supplemented with 2 mM glucose, 2 mM glutamine, 100 U/mL penicillin, 100 g/mL streptomycin, and 15% fetal bovine serum (FBS) (1640/15% FBS). Mouse breast cancer 4T1-luc and HEK-293 cells were obtained from the American Type Culture Collection (ATCC, Manassas, VA, USA) and maintained in DMEM (Invitrogen, Carlsbad, CA, USA) containing 10% FBS (Hyclone, Logan, UT, USA) and 50 U/mL penicillin-streptomycin. All cells were incubated at 37 °C in a humidified atmosphere with 5% CO₂.

The use of female BALB/c mice was approved in accordance with international ethical guidelines and the National Institutes of Health (NIH) Guide for the Care and Use of Laboratory Animals. Five-week-old female BALB/c mice were sourced from Shanghai

SLAC Laboratory Animal Co., Ltd. (Shanghai, China) and housed at the Experimental Animal Research Center of Zhejiang Chinese Medical University. All procedures followed NIH guidelines (Publication No. 85-23, revised 1996) for laboratory animal care and use.

2.2 Materials and reagents

Ursolic acid (UA) and doxorubicin (Dox) were obtained from Sigma-Aldrich Chemical (St. Louis, MO, USA). Matrigel was provided by BD Biosciences. Dulbecco's Modified Eagle's Medium (DMEM), fetal bovine serum (FBS), penicillin-streptomycin, and trypsin-EDTA were purchased from Invitrogen (Carlsbad, CA, USA). The BCA Protein Assay Kit was acquired from Beyotime. All antibodies were sourced from Cell Signaling Technology (CST, Beverly, MA, USA). Unless otherwise specified, additional reagents were obtained from Sigma-Aldrich.

2.3 Tube formation assay

The tube formation assay was used to evaluate the angiogenic potential of HUVECs. Matrigel (1:1 v/v) was thawed overnight at 4 °C, then plated onto the bottom of pre-chilled 24-well plates and incubated at 37 °C for 1 hour to allow gelation. HUVECs were collected by enzymatic detachment, counted and diluted to 2×10^5 cell/mL in low-serum medium (1% FBS) containing 20 ng/mL Vascular Endothelial Growth Factor (VEGF) and different concentrations of drugs. Then, HUVECs were seeded on Matrigel and incubated at 37 °C. Tube formation was observed starting from 8 h after cell seeding and branch points of the capillary-like tubes quantified were counted under light microscopy (50 × fields).

2.4 MTT assay for cell viability

Cell viability was assessed using the MTT (3-(4,5-dimethylthiazol-2-yl)-2,5-diphenyltetrazolium bromide) assay. 4T1 cells were seeded into 96-well plates at a density of 5×10^3 cells per well and

allowed to adhere overnight. Cells were then treated with various concentrations of ursolic acid (UA) (0, 20, 40, 60 μM) for 24, 48, or 72 hours. At each time point, 20 μL of 5 mg/mL MTT solution (Sigma-Aldrich, USA) was added to each well and incubated for 4 hours at 37 °C. Subsequently, the medium was removed, and 150 μL of DMSO was added to dissolve the formazan crystals. Absorbance was measured at 570 nm using a microplate reader (Bio-Rad, USA). Cell viability was expressed as a percentage relative to the untreated control.

2.5 Cell apoptosis assay by flow cytometry

Apoptosis was evaluated using an Annexin V-EGFP/PI double staining kit (KeyGEN Biotech, Nanjing, China) according to the manufacturer's instructions. Briefly, 4T1 cells were treated with UA (30 μM) for 24 hours, then harvested using trypsin without EDTA, washed twice with cold PBS, and resuspended in 500 μL of binding buffer. Cells were stained with 5 μL of Annexin V-EGFP and 5 μL of propidium iodide (PI) in the dark for 15 minutes at room temperature. The stained cells were analyzed immediately using flow cytometry (FACSCalibur, BD Biosciences). The results were interpreted as follows: Annexin V-/PI- (live cells), Annexin V+/PI- (early apoptosis), Annexin V+/PI+ (late apoptosis), and Annexin V-/PI+ (necrotic cells).

2.6 Cell cycle analysis

Cell cycle distribution was determined by propidium iodide (PI) staining. 4T1 cells were treated with UA (10 μM) for 48 hours, then harvested, washed twice with PBS, and fixed in 70% cold ethanol at 4 °C overnight. Fixed cells were washed again and incubated with PI/RNase staining solution containing 50 μg/mL PI and 100 μg/mL RNase A (Beyotime, China) for 30 minutes at room temperature in the dark. DNA content was analyzed using a flow cytometer (FACSCalibur, BD Biosciences), and cell cycle distribution (G0/G1, S, and G2/M phases) was evaluated using FlowJo software.

2.7 *In vivo* mice xenograft study

4T1-luc cells were treated with 0.25% trypsin and 0.02% EDTA for digestion, followed by centrifugation at $800 \times g$ to collect the cells. The cell pellets were resuspended at 1×10^7 cells/mL with phosphate-buffered saline (PBS), and 5×10^5 4T1-Luc cells in 100 μ L of PBS were injected into the mammary fat pad (MFP) of each mouse using 27 gauge needles. The animals were housed under standard conditions (12-hour light/dark cycle, controlled temperature of 22 ± 2 °C, and humidity of $50 \pm 5\%$) with ad libitum access to food and water. All animal experiments were performed following the guidelines approved by the Institutional Animal Care and Use Committee (IACUC). Mice were randomly divided into three groups (n = 6 per group): a model group (tumor-bearing mice receiving vehicle treatment), a UA-treated group (tumor-bearing mice administered ursolic acid at 10 mg/kg/day orally), and a Dox-treated group (tumor-bearing mice receiving doxorubicin at 1 mg/kg every other day via intraperitoneal injection) as a positive control. Tumor growth and metastases were monitored by bioluminescence imaging. At the endpoint of the experiment, mice were euthanized humanely by CO₂ inhalation according to institutional ethical standards.

2.8 *In vivo* bioluminescence imaging

Cell implantation and tumor growth were monitored using bioluminescence imaging (BLI) with an IVIS 200 imaging system (Caliper Life Sciences, Hopkinton, MA, USA). Mice were anesthetized with isoflurane and injected intraperitoneally with D-luciferin solution (Gold Biotechnology, St. Louis, MO, USA) at a dose of 100 mg/kg body weight in 0.1 mL of sterile PBS before imaging. Bioluminescence signals were quantified by determining the integrated flux of photons (photons per second) within each area of interest using Xenogen's Living Image V2.50.1 software. Mean \pm SE values of photon fluxes were calculated for each

experimental point according to time and treatment conditions.

2.9 High-resolution laser doppler perfusion imaging

Laser Doppler perfusion imaging was used to quantify microvascular perfusion in the upper dermis *in vivo*. This technique is based on the Doppler effect on monochromatic radiation caused by moving erythrocytes in the microvascular network. A laser beam was sequentially moved over the tissue surface, and reflections from moving blood cells were detected by a remote photodiode, converting the returning light into electrical impulses. The signal processor calculated a perfusion signal proportional to the tissue perfusion at each measurement point.

For this study, perfusion images were collected at selected sites: the tumor site (Flux 1), adjacent healthy skin surrounding the tumor (Flux 2), and the heart (Flux 3) in 4T1 tumor-bearing mice [19,20]. Imaging was performed under 1-2% isoflurane anesthesia, with mice maintained at normal body temperature using a circulating water heating pad. Ambient light conditions were standardized across all imaging sessions. To prevent artificial elevation of normal hemoglobin saturation, anesthesia was delivered using 21% oxygen instead of 100% oxygen.

A six-color scale (blue, green, yellow, and red) was used to generate color-coded perfusion images displayed on a monitor. The related perfusion values were calculated as follows:

$$\text{Tumor perfusion rate} = (F1/F3) \times 100\%$$

$$\text{Vascular perfusion rate} = (F2/F3) \times 100\%$$

2.10 Histopathological analysis and immunohistochemistry

Tumor and lung tissues were fixed in formalin, embedded in paraffin, and sectioned into 5 μ m slices. The sections were then deparaffinized in xylene and rehydrated through a graded series of alcohol to

distilled water. For histopathological analysis, sections were stained with hematoxylin for 5 minutes and eosin for 2 minutes. For immunohistochemistry analysis, the tissue sections were incubated overnight at 4 °C with primary antibodies against ICAM-1, integrin β 5, or ESM-1 (Santa Cruz Biotechnology) according to the manufacturer's protocol. The sections were then rinsed three times with PBS and incubated with a biotin-conjugated secondary antibody (Invitrogen) for 30 minutes at 37 °C, followed by three additional PBS washes. Horseradish peroxidase-labeled streptavidin was added and incubated at 37 °C for 30 minutes. The color reaction was developed using 3,3'-diaminobenzidine tetrahydrochloride (DAB), after which the slides were gently rinsed under running tap water. Finally, the sections were counterstained with hematoxylin, dehydrated, dried, and mounted for analysis.

2.11 Statistical analysis

All values are presented as the mean \pm standard deviation (SD) of four independent measurements. Statistical analysis was conducted using a two-tailed t -test, assuming two-sample unequal variance. A p -value of < 0.05 was considered statistically significant (* $p < 0.05$, ** $p < 0.01$).

3 Results

3.1 Ursolic acid suppresses breast cancer cell proliferation and metastasis

Ursolic acid (UA) significantly inhibited the proliferation of 4T1 breast cancer cells *in vitro*, demonstrated by the dose-dependent decrease in cell survival rates observed through the MTT assay at 24, 48, and 72 hours post-treatment (Figure 1A). Flow cytometry analysis revealed that UA treatment markedly increased apoptotic cells compared to untreated controls. Specifically, treatment with 30 μ M UA for 24 hours induced apoptosis in a substantial population of 4T1 cells, as indicated by increased Annexin V-EGFP and PI staining (Figure 1B). Additionally, cell cycle analysis showed that UA treatment (10 μ M for 48 hours) caused a significant arrest of 4T1 cells at the G1 phase, as evidenced by the accumulation of cells in the G1 phase compared with controls (Figure 1C). *In vivo* experiments further confirmed the inhibitory effects of UA on breast cancer growth and metastasis. Xenogen bioluminescence imaging showed that mice treated orally with UA at 20 mg/kg exhibited significantly reduced tumor growth compared to control mice after 3 and 4 weeks of treatment (Figure 1D). Collectively, these findings suggest that UA effectively suppresses breast cancer cell proliferation and induces apoptosis, alongside inhibiting tumor growth and metastasis *in vivo*.

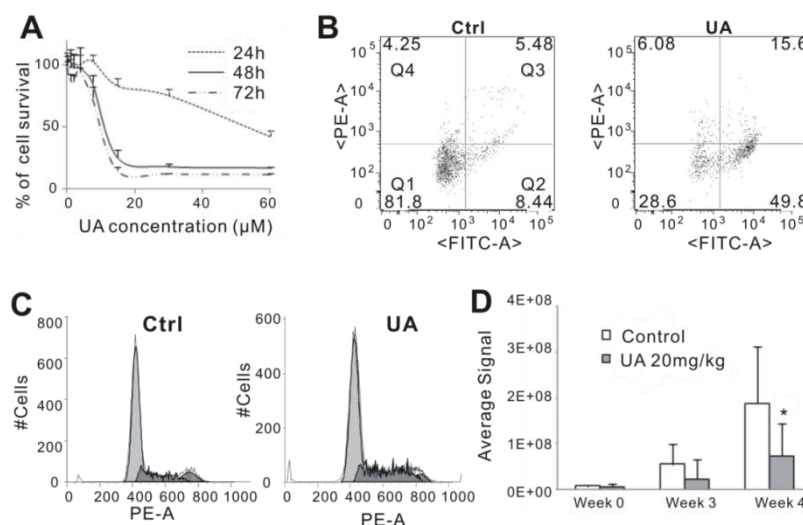


Figure 1 UA inhibits proliferation of breast cancer *in vitro* and *in vivo*. (A) MTT assay. 4T1 cells were treated with

different concentration of UA for 24, 48 or 72 hours. (B) Cell apoptosis assay. Quadrants: Q1 = live cells; Q2 & Q3 = apoptotic cells; Q4 = necrotic cells. (C) Cell cycle analysis. (D) Quantitative analysis of Xenogen imaging signal intensity (photons/sec/cm²/steradian) after 3 and 4 weeks treatment with UA. * $p < 0.05$.

3.2 UA inhibits tube formation of HUVECs

We investigated whether UA inhibits angiogenic functions regulated by endothelial cells. The formation of capillary-like structures by endothelial cells on a basement membrane matrix is a well-established method for assessing angiogenesis [18]. To evaluate the role of UA in this process, we conducted an *in vitro*

tube formation assay using human umbilical vein endothelial cells (HUVECs). HUVECs were incubated on Matrigel-coated plates, and tube formation was assessed after 8 hours. As shown in Figure 2, treatment with 10 μM UA resulted in a significant reduction in tube formation, with over a twofold decrease in loop number compared to the control (Figure 2).

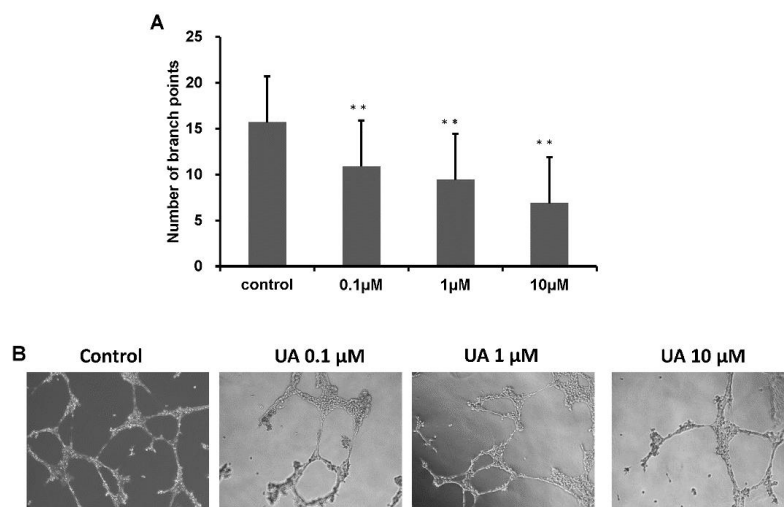


Figure 2 UA inhibits tube formation in HUVECs. (A) Quantification of endothelial branch points in a tube formation assay following treatment with VEGF alone (control) or VEGF in combination with UA at 0.1 μM , 1 μM , or 10 μM . Data are presented as mean \pm SD ($n = 6$). ** $p < 0.01$ vs. control. (B) Representative images of endothelial tube formation under the indicated treatment conditions. Magnification: 100 x.

3.3 UA inhibit tumor blood perfusion

Doppler perfusion imaging (LDPI) is a quantitative technique used for intravital analysis of blood perfusion changes. To assess perfusion dynamics in 4T1 tumor-bearing mice, LDPI was employed to evaluate blood flow in the tumor surface and the surrounding skin. The highest perfusion values were observed in the heart (red), while the tumor site exhibited low perfusion values (blue). Analysis of LDPI images revealed a reduction in abdominal perfusion

from week 3 (Figure 3), though no significant difference was observed between the UA-treated and model groups. These findings suggest that UA may slightly improve tumor necrosis four weeks after administration (Figure 3). However, the relative perfusion around the tumor site (Flux 2) in the UA group was significantly reduced to 82.54% of the model group ($p < 0.05$), indicating that UA markedly decreased local tumor blood perfusion three weeks after administration (Figure 3). This suggests that UA treatment effectively suppressed tumor angiogenesis.

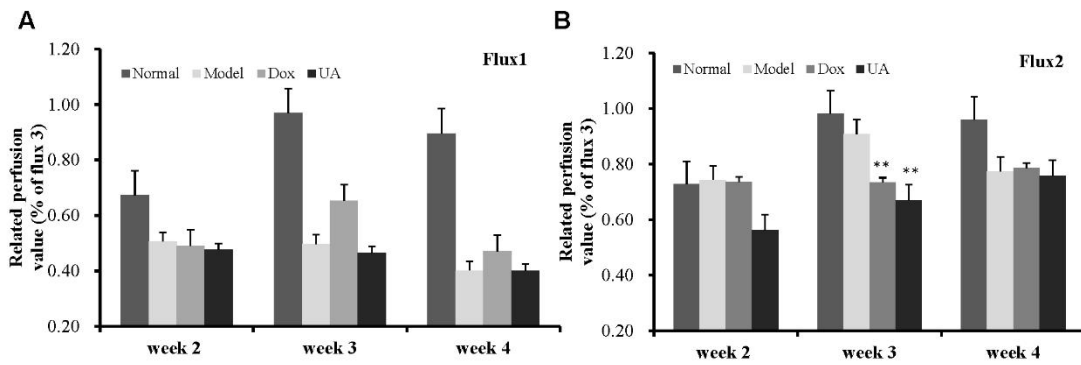


Figure 3 (A–B) UA inhibits *in vivo* blood perfusion in 4T1 tumor-bearing mice. three examined areas (1.4 * 1.4 cm) covered the tumor (Flux 1), adjacent healthy skin around tumor (Flux 2). Quantification of perfusion values (relative to normal control) measured at weeks 2, 3, and 4 post-treatment in two independent flux regions, Flux1 (A) and Flux2 (B). Groups include Normal, Model, Dox, and UA treatments.

3.4 UA inhibits *in vivo* tumor metastasis in mouse breast tumor model

To assess the anti-metastatic effect of UA *in vivo*, 4T1-Luc cells were orthotopically implanted into the mammary fat pads of BALB/c mice. UA was administered orally at 10 mg/kg/day, and doxorubicin (Dox, 1 mg/kg every other day) was used as a positive control. After 28 days of treatment, bioluminescence imaging revealed a marked reduction in tumor burden

in the UA-treated group compared to controls (Figure 4A). Histological examination of lung tissues by H&E staining showed a decreased number of metastatic foci in UA- and Dox-treated mice (Figure 4B). Furthermore, ICAM expression in lung sections was reduced in the UA-treated group, as revealed by immunohistochemistry (Figure 4C), suggesting a potential role of UA in suppressing adhesion molecule expression during metastasis.

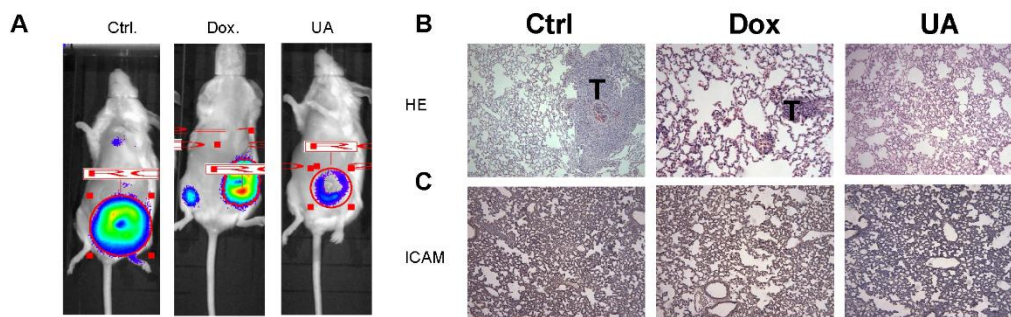


Figure 4 (A) Representative bioluminescence imaging of mice bearing 4T1-Luc tumors after 4 weeks of treatment with vehicle control (Ctrl), doxorubicin (Dox), or ursolic acid (UA). Regions of interest (ROI) indicate metastatic tumor burden. (B) Hematoxylin and eosin (H&E) staining shows metastatic tumor foci in the lungs (indicated as “T”). (C) Immunohistochemistry for ICAM demonstrates expression levels in lung tissues across different treatment groups. Magnification: 400 ×.

3.5 UA inhibits *in vivo* angiogenesis in 4T1 tumor bearing mice

Based on the *in vitro* findings, we next investigated the effects of UA on angiogenesis *in vivo* using the 4T1-luc tumor-bearing mouse model. Following oral

administration of UA and subsequent sacrifice of the mice, to further elucidate the underlying mechanism by which UA inhibits angiogenesis, we analyzed the expression of adhesion - and angiogenesis-related proteins, including integrin β 5, ESM-1, and ICAM-1, in the breast cancer tissue of mice (Figure 5).

Immunohistochemical staining demonstrated a substantial reduction in the expression of integrin β 5, ESM-1, and ICAM-1 in UA-treated tumors compared to the control group, supporting the role of UA in suppressing tumor angiogenesis.

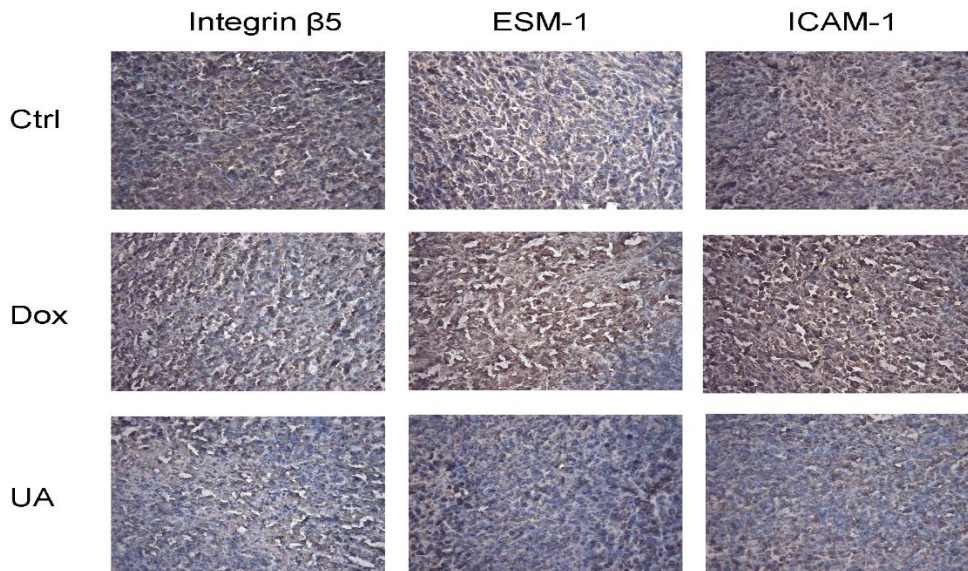


Figure 5 UA inhibits *in vivo* tumor angiogenesis in mouse breast cancer. Immunohistochemical staining of Integrin β 5, ESM-1, and ICAM-1 expression in control (Ctrl), Dox and UA-treated groups. Representative images show protein expression levels in the respective conditions. Magnification: 400 \times .

4 Discussion

In this study, we demonstrated that UA, a naturally occurring pentacyclic triterpenoid, exerts potent anti-metastatic and anti-angiogenic effects in a murine model of breast cancer. Consistent with previous reports highlighting UA's broad pharmacological activities, including anti-inflammatory and anti-tumor effects, our data provide new mechanistic insights into its role in regulating endothelial function and suppressing tumor progression [9,21-23].

Angiogenesis is a critical step in tumor development and metastasis, and targeting endothelial cells remains a promising therapeutic approach [24,25]. Inhibiting angiogenesis has emerged as an effective strategy in treating various solid tumors, and

anti-angiogenic agents such as bevacizumab have been incorporated into clinical regimens for breast and colorectal cancers [26]. However, such therapies often face challenges-including acquired resistance due to activation of alternative pro-angiogenic pathways, and off-target toxicities such as hypertension, bleeding, and thromboembolism [27]. Our *in vitro* data showed that UA significantly inhibited the proliferation of 4T1 cells and tube formation in HUVECs. *In vivo*, laser Doppler perfusion imaging revealed a marked decrease in tumor-associated blood perfusion following UA administration, further supporting its anti-angiogenic effect.

Our *in vitro* data demonstrated that UA significantly inhibited 4T1 cells proliferation, and endothelial cells tube formation. These anti-angiogenic effects may

potentially involve modulation of the ERK and NF- κ B signaling pathways. Since the ERK/MAPK pathway is a well-established downstream effector of VEGF signaling that promotes endothelial proliferation and angiogenesis [28,29]. UA-mediated suppression of this pathway could contribute to its inhibitory effects. Additionally, the NF- κ B pathway may also be involved, either as part of a compensatory stress response or through direct regulation, as has been reported in other cell types [30]. These possible mechanisms warrant further validation through pathway-specific inhibition or genetic approaches.

In vivo, laser Doppler perfusion revealed significantly decreased local tumor perfusion after UA administration, supporting the functional relevance of angiogenesis inhibition. Histological analysis further confirmed the anti-metastatic activity of UA in reducing lung metastatic foci in 4T1 tumor-bearing mice. Notably, UA downregulated several key adhesion molecules-ICAM-1, integrin β 5, and ESM-1-which are involved in endothelial cell adhesion, vascular permeability, and tumor extravasation. These molecules also play roles in establishing pre-metastatic niches and facilitating interactions between circulating tumor cells and vascular endothelium. Therefore, UA's simultaneous targeting of angiogenesis and adhesion likely contributes synergistically to its anti-metastatic efficacy.

Compared with conventional chemotherapy agents like doxorubicin, which often cause systemic toxicity and non-selective cytotoxicity, UA appears to act through a distinct mechanism that targets the tumor microenvironment rather than tumor cells alone. This feature may provide a therapeutic window for combining UA with standard therapies to enhance efficacy while minimizing toxicity.

Nevertheless, several limitations of this study should be acknowledged. First, the precise upstream regulators of UA's action remain to be fully elucidated,

particularly in relation to its dual modulation of ERK and NF- κ B signaling. Second, although our model focuses on breast cancer, the applicability of UA to other solid tumors requires validation. Lastly, pharmacokinetic data such as bioavailability, metabolism, and tissue distribution of UA *in vivo* were not addressed in this study and should be explored in future preclinical trials to assess translational feasibility.

In conclusion, our study identifies UA as a promising candidate for inhibiting breast cancer metastasis by targeting both angiogenesis and endothelial-tumor adhesion mechanisms. These findings underscore the therapeutic potential of naturally derived compounds in modulating the tumor microenvironment and provide a foundation for future investigations into UA-based combination therapies or structural analog development.

5 Conclusion

Our findings demonstrate that ursolic acid effectively suppresses breast cancer metastasis through the inhibition of angiogenesis and endothelial cell function. Mechanistically, UA reduces the expression of key adhesion molecules, limiting tumor vascularization and dissemination. These results suggest that UA may serve as a promising candidate for adjunctive therapy in metastatic breast cancer, particularly in strategies targeting the tumor vasculature and microenvironment. Further studies are warranted to optimize UA delivery, assess its long-term efficacy, and explore its potential in combination with current standard-of-care treatments.

Acknowledgements

Not applicable.

Conflicts of Interest

The authors declare no conflicts of interest.

Author Contributions

X.J.: Project design, Project administration, Methodology, Writing - original draft; K.H.: Conceptualization, Funding acquisition, Writing - review & editing.

Ethics Approval and Consent to Participate

All animal experiments were approved by the Ethics Committee of Hangzhou City University (No. 15725).

Funding

This study was supported by the Zhejiang Provincial Natural Science Foundation of China (LY19H280010).

Availability of Data and Materials

Data supporting this study are included within the article.

Supplementary Materials

Not applicable.

References

- [1] American Cancer Society. *Cancer Facts & Figures* 2025. American Cancer Society; 2025.
- [2] Loibl S, Poortmans P, Morrow M, et al. Early breast cancer: ESMO Clinical Practice Guideline for diagnosis, treatment and follow-up. *Annals of Oncology* 2024; 35(2): 159-182.
- [3] Gradishar WJ, Moran MS, Abraham J, et al. Breast Cancer, Version 3.2024, NCCN Clinical Practice Guidelines in Oncology. *Journal of the National Comprehensive Cancer Network* 2024; 22(5): 331-357.
- [4] Welt A, Ritter C, Kümmel S, et al. Improved survival in metastatic breast cancer: results from a 20-year study involving 1033 women treated at a single comprehensive cancer center. *Journal of Cancer Research and Clinical Oncology* 2020; 146(6): 1559-1566.
- [5] Greenberg PA, Hortobagyi GN, Smith TL, et al. Long-term follow-up of patients with complete remission following combination chemotherapy for metastatic breast cancer. *Journal of Clinical Oncology* 1996; 14(8): 2197-2205.
- [6] Jones SE. Metastatic Breast Cancer: The Treatment Challenge. *Clinical Breast Cancer* 2008; 8(3): 224-233.
- [7] Weis SM, Cheresch DA. Tumor angiogenesis: molecular

pathways and therapeutic targets. *Nature Medicine* 2011; 17(11): 1359-1370.

[8] Liu ZL, Chen HH, Zheng LL, et al. Angiogenic signaling pathways and anti-angiogenic therapy for cancer. *Signal Transduction and Targeted Therapy* 2023; 8(1): 198.

[9] Ikeda Y, Murakami A, Ohigashi H. Ursolic acid: an anti- and pro-inflammatory triterpenoid. *Molecular Nutrition & Food Research* 2008; 52(1): 26-42.

[10] Iqbal J, Abbasi BA, Mahmood T, et al. Ursolic acid a promising candidate in the therapeutics of breast cancer: Current status and future implications. *Biomedicine & Pharmacotherapy* 2018; 108: 752-756.

[11] Wang S, Wang N, Tan HY, et al. Ursolic Acid Inhibits Breast Cancer Metastasis by Suppressing Glycolytic Metabolism via Activating SP1/Caveolin-1 Signaling. *Frontiers in Oncology* 2021; 11: 745584.

[12] Chan EWC, Wong SK, Chan HT. Ursolic acid: An overview on its cytotoxic activities against breast and colorectal cancer cells. *Journal of Integrative Medicine* 2019; 17(3): 155-160.

[13] Yin R, Li T, Tian JX, et al. Ursolic acid, a potential anticancer compound for breast cancer therapy. *Critical Reviews in Food Science and Nutrition* 2018; 58(4): 568-574.

[14] Sohn KH, Lee HY, Chung HY, et al. Anti-angiogenic activity of triterpene acids. *Cancer Letters* 1995; 94(2): 213-218.

[15] Cárdenas C, Quesada AR, Medina MA. Effects of ursolic acid on different steps of the angiogenic process. *Biochemical and Biophysical Research Communications* 2004; 320(2): 402-408.

[16] Gao JL, Shi JM, He K, et al. Tetrandrine Suppresses Cancer Angiogenesis and Metastasis in 4T1 Tumor Bearing Mice. *Evidence-Based Complementary and Alternative Medicine* 2013; 2013: 265061.

[17] Bell R, Barraclough R, Vasieva O. Gene Expression Meta-Analysis of Potential Metastatic Breast Cancer Markers. *Current Molecular Medicine* 2017; 17(3): 200-210.

[18] Fisher B, Bauer M, Wickerham DL, et al. Relation of number of positive axillary nodes to the prognosis of patients with primary breast cancer. An NSABP update. *Cancer* 1983; 52(9): 1551-1557.

[19] Scholz D, Cai WJ, Schaper W. Contribution of arteriogenesis and angiogenesis to postocclusive hindlimb perfusion in mice. *Journal of Molecular and Cellular Cardiology* 2002; 34(7): 775-787.

- [20] Poole KM, Nelson CE, Joshi RV, et al. Quantitative optical imaging of vascular response in vivo in a model of peripheral arterial disease. *American Journal of Physiology-Heart and Circulatory Physiology* 2013; 305(8): H1168-H1180.
- [21] Khwaza V, Oyedeji OO, Aderibigbe BA. Ursolic Acid-Based Derivatives as Potential Anti-Cancer Agents: An Update. *International Journal of Molecular Sciences* 2020; 21(16).
- [22] Kornel A, Nadile M, Retsidou MI, et al. Ursolic Acid against Prostate and Urogenital Cancers: A Review of In Vitro and In Vivo Studies. *International Journal of Molecular Sciences* 2023; 24(8).
- [23] Sandhu SS, Kumar R, Abbas M, et al. Ursolic acid: a pentacyclic triterpenoid that exhibits anticancer therapeutic potential by modulating multiple oncogenic targets. *Biotechnology and Genetic Engineering Reviews* 2023; 39(2): 729-759.
- [24] Lugano R, Ramachandran M, Dimberg A. Tumor angiogenesis: causes, consequences, challenges and opportunities. *Cellular and Molecular Life Sciences* 2020; 77(9): 1745-1770.
- [25] Apte RS, Chen DS, Ferrara N. VEGF in Signaling and Disease: Beyond Discovery and Development. *Cell* 2019; 176(6): 1248-1264.
- [26] Chen H, Zhang L, Wang Y, et al. Advances in bevacizumab in colorectal cancer: a bibliometric analysis from 2004 to 2023. *Frontiers in Oncology* 2025; 15.
- [27] Shord SS, Bressler LR, Tierney LA, et al. Understanding and managing the possible adverse effects associated with bevacizumab. *American Journal of Health-System Pharmacy* 2009; 66(11): 999-1013.
- [28] Okuda KS, Hogan BM, Hall CJ, et al. Live-imaging of endothelial Erk activity reveals dynamic and sequential signalling events during regenerative angiogenesis. *eLife* 2021; 10: e62196.
- [29] Song YY, Li XH, Li YQ, et al. The role of the ERK signaling pathway in promoting angiogenesis for treating ischemic diseases. *Frontiers in Cell and Developmental Biology* 2023; 11.
- [30] Shishodia S, Majumdar S, Banerjee S, et al. Ursolic acid inhibits nuclear factor-kappaB activation induced by carcinogenic agents through suppression of IkappaBalpha kinase and p65 phosphorylation: correlation with down-regulation of cyclooxygenase 2, matrix metalloproteinase 9, and cyclin D1. *Cancer Research* 2003; 63(15): 4375-4383.